Supplementary Information (SI) for Chemical Science.

Supplementary Information

Dual Role of a Conjugated Bridge in Intramolecular Singlet Fission: Light-Harvesting Antenna and Energy Funnel

Jie Kong[1], Kanad Majumder[2], Manoj K. Sharma[2], Soham Mukherjee[3], Andrew J. Musser[3], Satish Patil[2,*], Woojae Kim[1,*]

[1]Department of Chemistry, Yonsei University, Seoul 03722, Republic of Korea.

[2]Solid State and Structural Chemistry Unit, Indian Institute of Science, Bengaluru-560012, India.

[3]Department of Chemistry and Chemical Biology, Cornell University, Ithaca, NY 14850, USA.

Correspondence to: spatil@iisc.ac.in, woojae@yonsei.ac.kr

Table of Contents

S1. Materials and Methods

1. Materials

The chemicals HEX, THF, TOL, BZN, pyridine, anthracene, zinc phthalocyanine and Rhodamine 6G were bought from Sigma-Aldrich, 6,13-bis(triisopropylsilylethynyl)pentacene (P) was purchased from Ossila, and was used directly without further purification. All solvents were dried by standard methods. Chemicals were purchased from Aldrich, Acros Organics, S.D. fine chemicals, B.L.D. Pharm, T.C.I. India and Spectrochem and used without further purification. Compound xx were synthesized via reported procedures as described later. THF was distilled from sodium/benzophenone ketyl. Anhydrous Na_2SO_4 was used as the drying agent after aqueous work-up. Evaporation and concentration in vacuo were done at water aspirator pressure. All reactions were performed in standard, dry glassware under an inert atmosphere of nitrogen or argon. Column chromatography: silica gel-60 (230–400 mesh). Thin Layer Chromatography (TLC): precoated plastic sheets covered with 0.20 mm silica gel with fluorescent indicator UV 254 nm; visualization by UV light. Detailed synthesis procedures are provided in Supplementary Information Section 2.

2. Theoretical Calculations

Structural optimization and energy level were performed based on the DFT and TD-DFT by employing the Gaussian 16, Revision C.01 package.[1] Optimization of the S_0 state geometries were obtained using the CAM-B3LYP functional[2] at the basis set 6-311g(d,p) level.[3] The FMOs and electron-hole analysis were performed by using the Multiwfn[4] and VMD softwares[5] based on the Gaussian outputs.

3. Steady-State Absorption and Photoluminescence

The optical absorption spectra were recorded with a JASCO V-770 spectrometer at room temperature. Photoluminescence (PL) spectra were carried out on an F-7000 spectrometer from Hitachi. PL spectra are spectrally corrected by using a correction factor of the spectrophotometer. The PL quantum yields (PLQY) were measured by applying the comparative method with rhodamine-6G as the reference (solvent: ethanol, excitation wavelength: 488 nm, PLQY: 94%) and zinc phthalocyanine as the reference (solvent: pyridine, excitation wavelength: 650 nm, PLQY: 30%).[6]

4. Time-resolved Photoluminescence Measurements

The time-resolved PL measurements were performed with an ICCD detector (PI-MAX4, Princeton Instruments) after photoexcitation using 400 pump (170 fs) generated through an optical parametric amplifier (OPA, ORPHEUS, Light Conversion) and its second harmonic (SH, LYRA-SH, Light Conversion) module, pumped by a Yb:KGW amplifier (PHAROS-SP-1.5mJ, Light Conversion, 1030 nm, 600 μJ, 10 kHz, 176 fs). The system had an instrumental response function of 500 ps.

5. Electrochemical measurements

Cyclic voltammetry (CV) was carried out on Autolab potentiostat in a custom-made electrochemical cell using Platinum disc (3 mm diameter) as the working electrode, platinum coil as the counter electrode, and Ag^+/Ag nonaqueous reference electrode in 0.1 M TBAPF6 electrolyte in DCM solvent. The reference electrode was prepared by dipping a silver wire in a glass tube of 10 mM silver triflate (AgOTf) in 0.1 M of DCM-TBAPF6 as a fill solution. The reference electrode was calibrated each time before the start of experiments against ferrocene ($E_{1/2}$ = 180 (±10) mV. The electrochemical cell was sealed and purged with Ar gas for 15 min before experiments. The scan rate was maintained at 50 mV/s for every experiment.

$$E_{HOMO}\ (eV) = -4.8 - (E_{onset,ox} - E_{1/2,Fc/Fc+}) \qquad E_{LUMO}\ (eV) = -4.8 - (E_{onset,red} - E_{1/2,Fc/Fc+})$$

6. Femtosecond Transient Absorption Measurements

A Ti:Sapphire regenerative amplifier system (800 nm, 350 μJ, 10 kHz, 35 fs, Spitfire Pro, Spectra Physics) was used as a fundamental laser source for a femtosecond transient absorption (fs-TA) spectrometer. First, fundamental pulses were divided into two parts by a 5:5 (R:T) beam splitter. A half portion of fundamental pulses consisted of optical parametric amplifiers (TOPAS C, Spectra Physics). The other portion was attenuated by a combination of irises and a neutral density filter, and used to generate white-light continuum (WLC) probe pulses via a 4 mm calcium fluoride window (EKSMA Optics). The time delay between the pump and probe beams was controlled by a linear motor stage (ILS300LM-S, Newport) on the beamline for probe generation. Spectra of the dispersed WLC probe are monitored by a high-speed spectrometer (Ultrafast Systems). Due to the camera's frame rate limit, we obtained TA spectra at 2 kHz. For this, the pump pulses were modulated at 1 kHz using an optical chopper (MC2000B for the controller, MC1F10 for the optical chopper blade, Thorlabs). Thus, the detection procedure involves measuring five consecutive laser pulses to produce a single TA spectrum. To prevent polarization-dependent signals, the polarization angle of the pump pulse was set at the magic angle (54.7°) to the horizontally polarized probe pulse using a Glan-laser calcite polarizer (GL10-A, Thorlabs) and an achromatic half-wave plate (AQWP05M-600, Thorlabs). The pump wavelengths for P-PDPP and P-PDPP-P are 480 nm and 600 nm. The samples were measured in a 2 mm quartz cell, the concentrations are 10^{-5} M for both samples, and absorption spectra were consistently checked after each experiment to confirm no photo-degradation. Both fs-TA and ns-TA results were analyzed using Glotaran software.[7]

7. Nanosecond Transient Absorption Measurements

Nanosecond transient absorption spectroscopy (ns-TA) experiments were performed using a commercial spectrometer (EOS, Ultrafast Systems). The excitation pulses were generated by a commercial collinear optical parametric amplifier (ORPHEUS, Light Conversion) combined with a second-harmonic generation stage (LYRA-SH, Light Conversion). The a Yb:KGW regenerative amplifier (PHAROS-SP-1.5mJ, Light Conversion, 1030 nm, 600 μJ, 10 kHz, 176 fs) was used as the main source for ns-TA.

The excitation wavelengths for **P-PDPP** and **P-PDPP-P** are 480 and 600 nm. For the anthracene-sensitized experiments, the excitation wavelength is 360 nm. The oxygen in solutions was removed by degassing with argon gas for 15 min. All measurements were carried out at room temperature. The samples were measured in a 2 mm quartz cell. The absorption spectra were consistently checked after each experiment to confirm no photo-degradation.

8. Calculation on FRET for P-PDPP

Quantitative FRET calculations[8, 9] were performed to further substantiate the assignment of the PDPP to the pentacene energy-transfer mechanism and to rationalize the solvent-dependent kinetics observed experimentally. The FRET rate constants were evaluated using the standard Förster formalism, incorporating the experimentally determined donor fluorescence quantum yield, solvent refractive index, the calculated orientation factor κ^2, and the spectral-overlap integral J, derived from the overlap between the PDPP emission and pentacene absorption spectra. Transition dipole orientations were obtained from optimized molecular geometries and TD-DFT calculations. For **P-PDPP**, the donor–acceptor separation was determined to be approximately 13.3 Å, and the orientation factor κ^2 was calculated to be ~1.15, reflecting a favorable relative alignment of the PDPP emission dipole and the pentacene absorption dipole. The resulting Förster radius R_0 substantially exceeds the donor–acceptor separation, leading to calculated energy-transfer efficiencies approaching unity.

$$R_0 = 0.02108\left(\frac{\kappa^2 \phi_D J}{n^4}\right)^{1/6}$$

$$J = \int_{\lambda_1}^{\lambda_2} F_D\,(\lambda)\varepsilon_A(\lambda)\lambda^4 d\lambda$$

$$k_{FRET} = \frac{1}{\tau_D}\left(\frac{R_0}{R_{DA}}\right)^6$$

$$E = \frac{1}{1+\left(\frac{R_{DA}}{R_0}\right)^6}$$

Where Φ_D is the fluorescence quantum yield of the donor in the absence of acceptor, n is the refractive index of the medium, R_{DA} is the donor–acceptor distance, E is FRET efficiency, τ_D is lifetime of the donor without acceptor, F_D is the area normalized emission of the donor, and ε_A is the extinction coefficient of the acceptor. The integral J is called the spectral overlap integral and can be seen as the energy match between the two states involved in the energy transfer process.

The spectral-overlap integral J increases systematically with solvent polarity due to the red shift of PDPP emission and the corresponding enhancement of overlap with pentacene absorption. In toluene and benzonitrile, J values are comparable owing to the quadrupolar nature of toluene, which produces PDPP emission spectra similar to those in benzonitrile. Calculated FRET rates reproduce both the magnitude and the solvent-dependent trend of the experimentally extracted rates, with minor deviations in highly polar solvents attributable to limitations in the treatment of solvent refractive index. For **P-PDPP-P**, the presence of two pentacene acceptor units leads to an approximately two-fold increase in the effective acceptor absorption coefficient, resulting in a corresponding increase in J and a substantially enhanced FRET rate, consistent with the experimentally observed acceleration of PDPP→ pentacene energy transfer in the dimeric architecture.

S2. Synthesis and Characterization

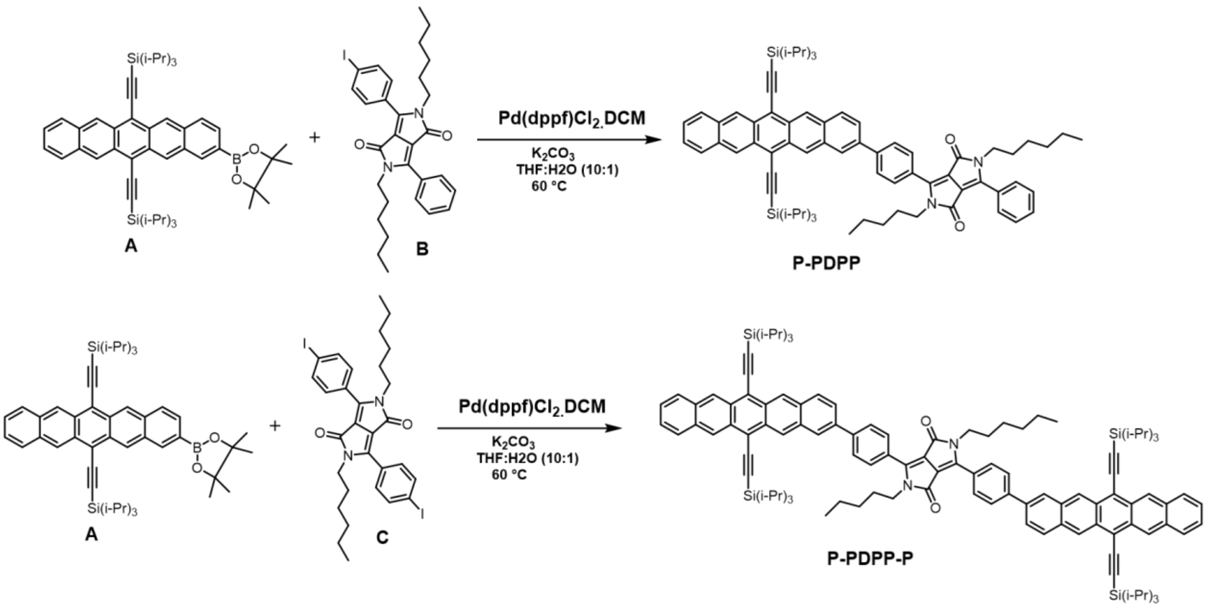

Scheme S1. Synthetic scheme for **P-PDPP** and **P-PDPP-P**. All three monomers were synthesized according to the procedure reported in the literature.[10, 11]

Synthesis of P-PDPP:

To a dry round-bottom flask were added 2,5-dihexyl-3-(4-iodophenyl)-6-phenyl-2,5 dihydropyrrolo[3,4-c]pyrrole-1,4-dione (**B**, 100 mg, 0.171 mmol, 1.0 equiv), 6,13-bis(triisopropylsilylethynyl) pentacene, (**A**, 145 mg, 0.189 mmol, 1.1 equiv), K_2CO_3 (17 equiv), and $Pd(dppf)_2Cl_2 \cdot DCM$ (0.1 equiv). The reaction mixture was degassed by successive vacuum–argon cycles, followed by the addition of degassed THF/H_2O (10:1, v/v, 15 mL). The resulting mixture was heated at reflux (60 °C) overnight in the dark. After cooling to room temperature, the solvents were removed under reduced pressure, and the crude product was purified by silica gel column chromatography using hexanes/dichloromethane mixtures as the eluent to obtain the product (135 mg, yield 72%) as a purple solid.

^{1}H NMR (400 MHz, $CDCl_3$) δ 9.39-9.34 (m,4H), 8.26 (s,1H), 8.13-8.11 (d,1H), 8.07-8.00 (m, 6H), 7.88-7.86 (d,2H), 7.79-7.77 (d,2H), 7.58-7.57 (m,3H), 7.47-7.44 (m,2H), 3.90-3.77 (m,4H), 1.72-1.64 (m,4H), 1.50-1.30 (m,42H), 1.30-1.25 (m,12H), 0.95-0.80 (m,6H). ^{13}C NMR (125 MHz, $CDCl_3$) δ 162.83, 162.81, 148.47, 148.10, 143.33, 137.03, 132.40, 132.25, 131.52, 131.12, 130.97, 130.90, 130.81, 130.71, 129.73, 129.41, 128.91, 128.74, 128.70, 128.32, 127.56, 127.40, 127.05, 126.57, 126.42, 126.37, 126.30, 126.13, 125.71, 118.54, 118.47, 110.02, 109.90, 107.54, 107.33, 104.63, 42.14, 42.05, 42.04, 41.99, 31.27, 31.24, 29.71, 29.52, 29.43, 26.47, 26.42, 22.52, 22.47, 19.05, 19.03, 13.99, 13.96, 11.71. MALDI-TOF MS m/z calcd. for $C_{74}H_{88}N_2O_2Si_2$ (M^+) 1092.638, found 1092.729 (M^+).

Synthesis of P-PDPP-P:

To a dry round-bottom flask were added 2,5-dihexyl-3,6-bis(4-iodophenyl)-2,5-dihydropyrrolo[3,4-c]pyrrole-1,4-dione (**C,** 125 mg, 0.176 mmol, 1.0 equiv), 6,13-bis(triisopropylsilylethynyl) pentacene (**A,** 337 mg, 0.441 mmol, 2.5 equiv), K_2CO_3 (17 equiv), and Pd(dppf)$_2$Cl$_2$·DCM (0.1 equiv). The reaction mixture was degassed by successive vacuum–argon cycles, followed by the addition of degassed THF/H_2O (10:1, v/v, 15 mL). The resulting mixture was heated at reflux (60 °C) overnight in the dark. After cooling to room temperature, the solvents were removed under reduced pressure, and the crude product was purified by silica gel column chromatography using hexanes/dichloromethane mixtures as the eluent to obtain the product (180 mg, yield 59%) as a dark purple solid.

^{1}H NMR (500 MHz, $CDCl_3$) δ 9.36-9.30 (m,8H), 8.23 (s,2H), 8.09-8.07 (d,2H), 8.06-8.04 (d, 4H), 7.99-7.96 (d,8H), 7.76-7.74 (d,2H), 7.43-7.41 (m,4H), 3.91-3.88 (m,4H), 1.74-1.71 (m,4H), 1.42-1.34 (m,84H), 1.30-1.24 (m,12H), 0.88-0.84 (m,6H). ^{13}C NMR (125 MHz, $CDCl_3$) δ163.00, 148.13, 143.43, 137.10, 132.48, 132.46, 132.31, 131.59, 131.04, 130.97, 130.88, 130.79, 129.82, 129.53, 128.78, 127.65, 127.47, 127.14, 126.67, 126.50, 126.46, 126.37, 126.21, 125.78, 118.62, 118.54, 110.23, 107.61, 107.40, 104.71, 104.67, 42.30, 31.37, 29.78, 29.63, 26.58, 22.61, 19.13, 19.10, 14.09, 11.78. MALDI-TOF MS m/z calcd. for $C_{118}H_{140}N_2O_2Si_4$ (M^+) 1730.003, found 1729.330 M-1).

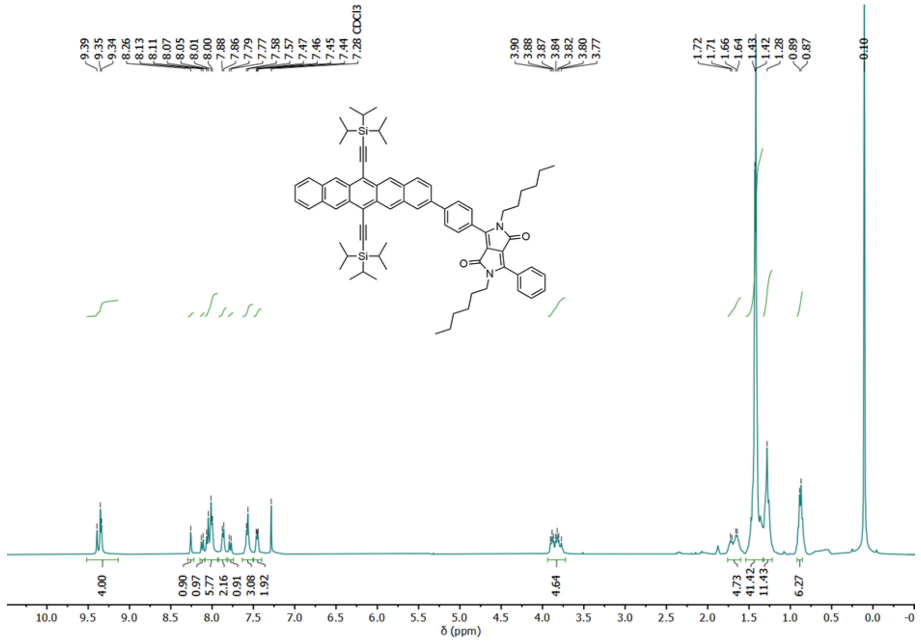

Fig. S1. ^{1}H-NMR of **P-PDPP** in $CDCl_3$.

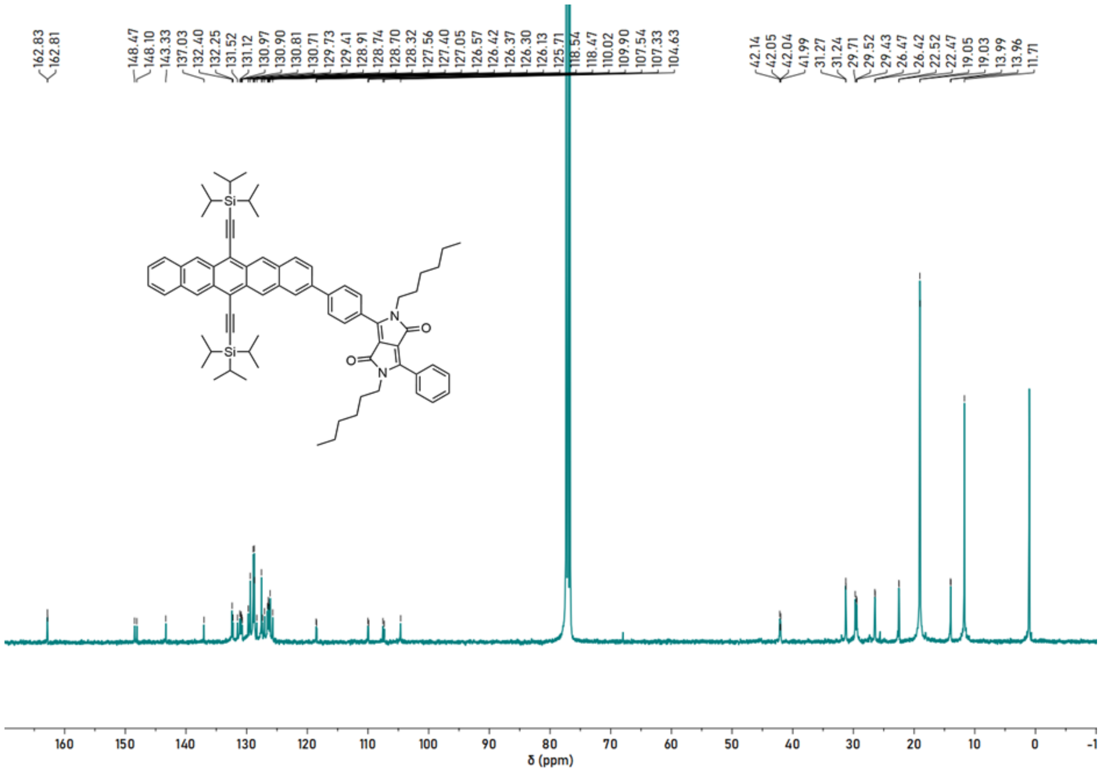

Fig. S2. $^{13}C\{1H\}$ -NMR of **P-PDPP** in $CDCl_3$.

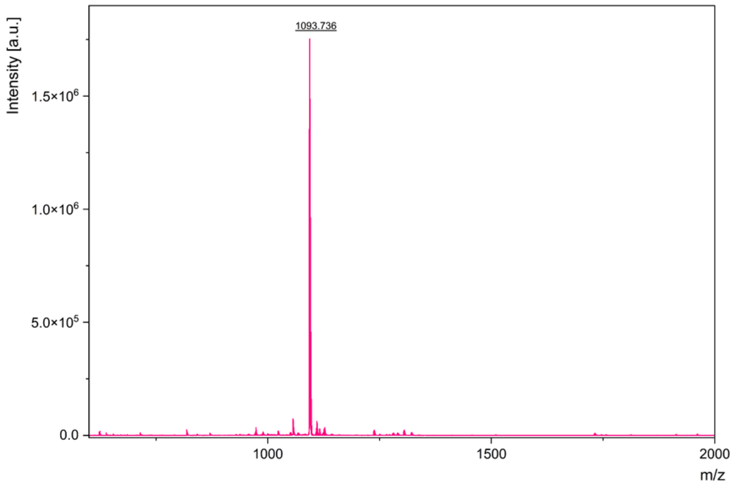

Fig. S3. MALDI-MS of **P-PDPP**.

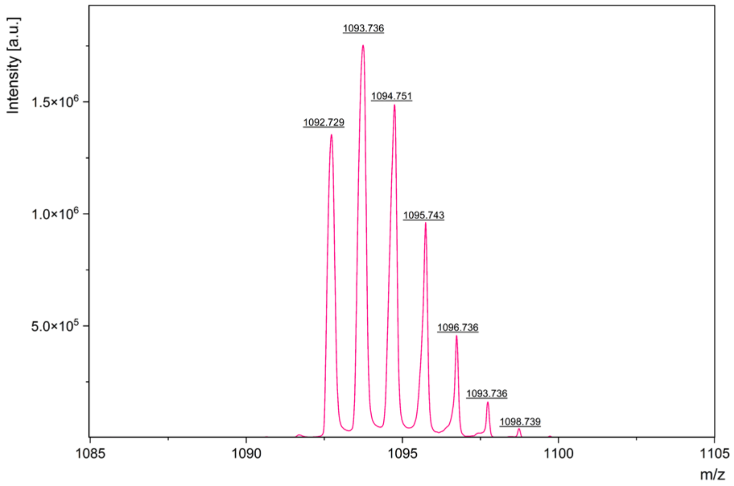

Fig. S4. MALDI-MS isotopic distribution of **P-PDPP**.

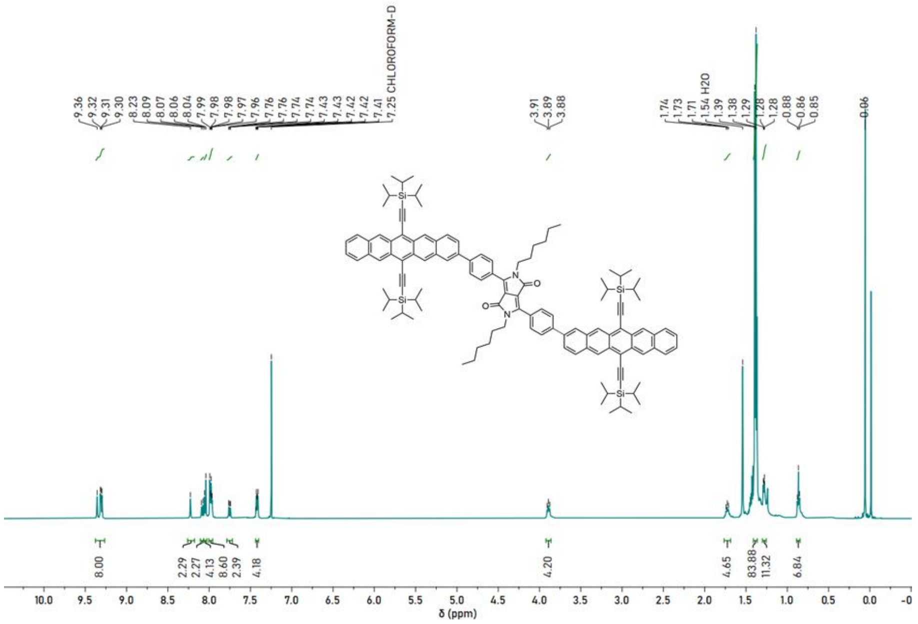

Fig. S5. ^{1}H-NMR of **P-PDPP-P** in CDCl$_3$.

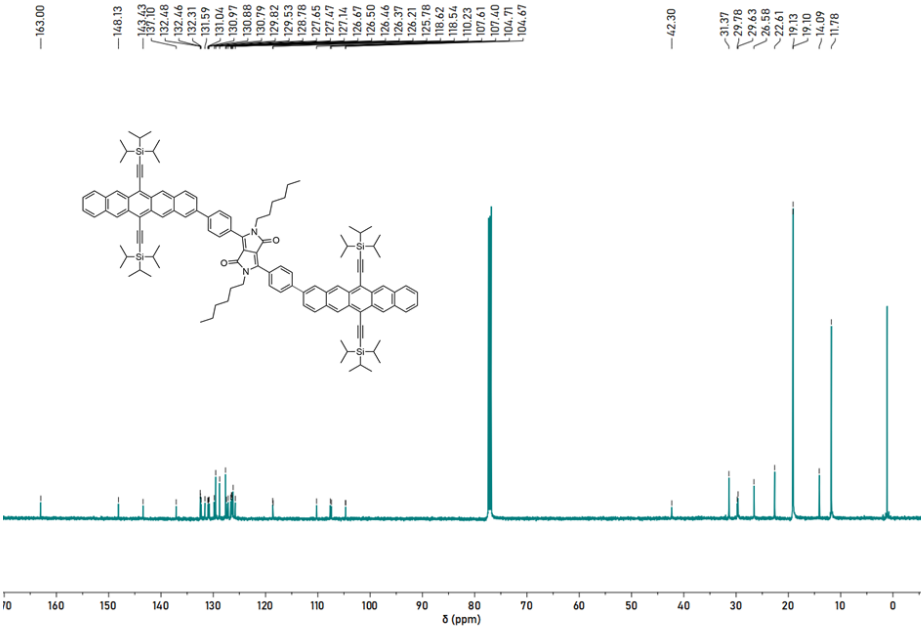

Fig. S6. ^{13}C*{1H}*-NMR of **P-PDPP-P** in CDCl$_3$.

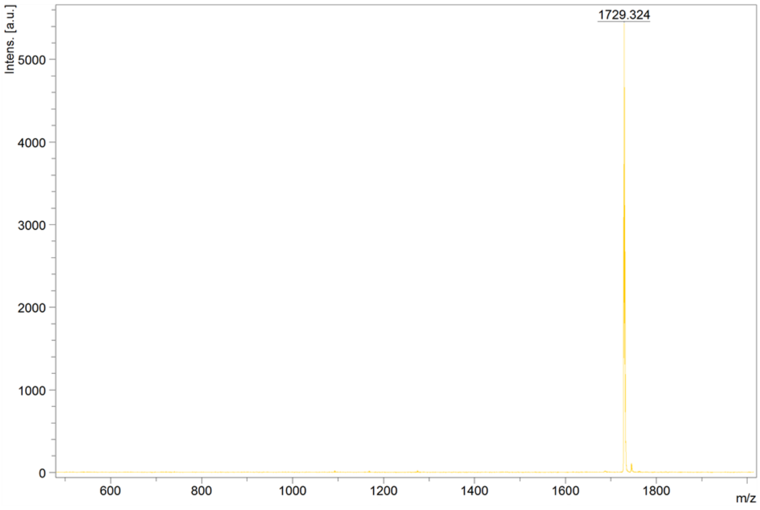

m/z	S/N	Quality Fac.	Res.	Intens.	Area
1729.324				5441	
1730.320	571		730	4663	11084

Fig. S7. MALDI-MS of **P-PDPP-P**.

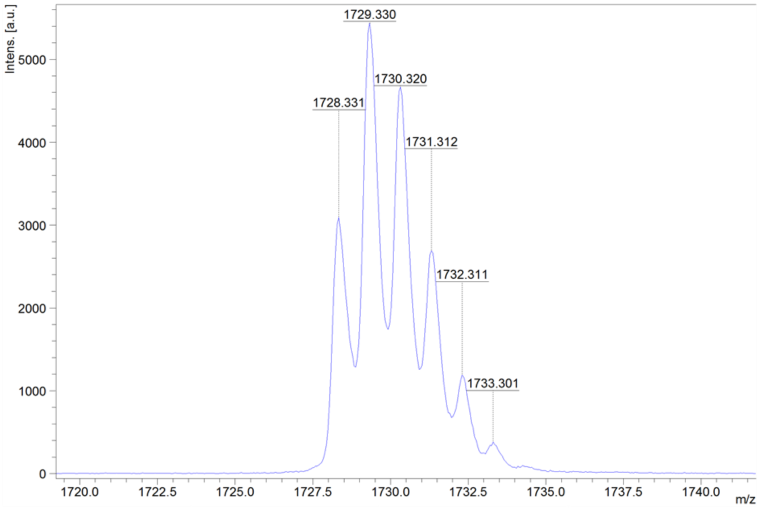

m/z	S/N	Quality Fac.	Res.	Intens.	Area
1728.331				3093	
1729.330				5425	
1730.320	571		730	4663	11084
1731.312				2690	
1732.311				1189	
1733.301				381	

Fig. S8. MALDI-MS isotopic distribution of **P-PDPP-P**.

S3. Steady-State Spectra

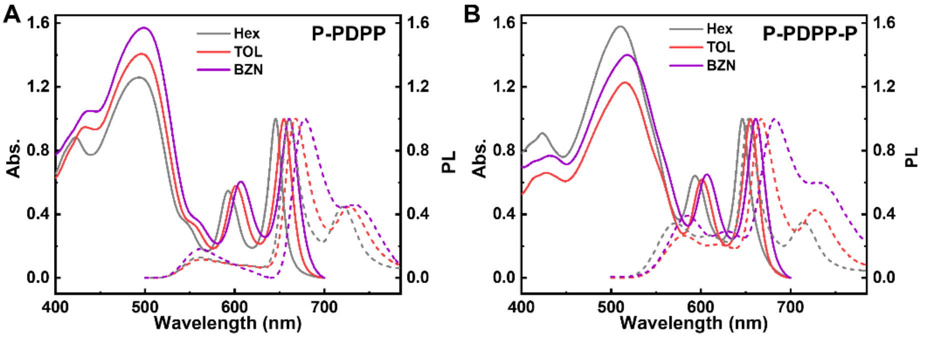

Fig. S9. Steady-state absorption and PL spectra of (A) **P-PDPP** and (B) **P-PDPP-P** in different solvents.

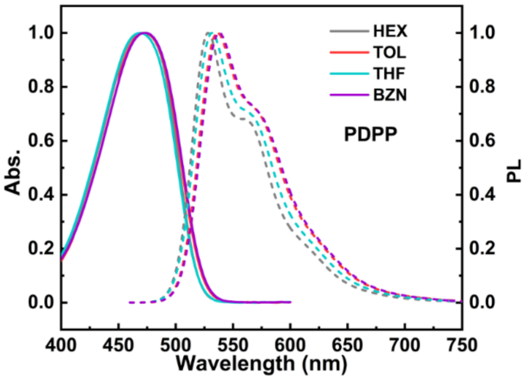

Fig. S10. Steady-state absorption and PL spectra of PDPP in different solvents.

Table S1. The molar extinction coefficient values of P, PDPP, **P-PDPP** and **P-PDPP-P** in THF.

	ε (PDPP, $M^{-1}cm^{-1}$)	**ε (P, $M^{-1}cm^{-1}$)**
PDPP	$1.69*10^4$	/
P	/	$2.59*10^4$
P-PDPP	$3.21*10^4$	$2.31*10^4$
P-PDPP-P	$4.86*10^4$	$4.05*10^4$

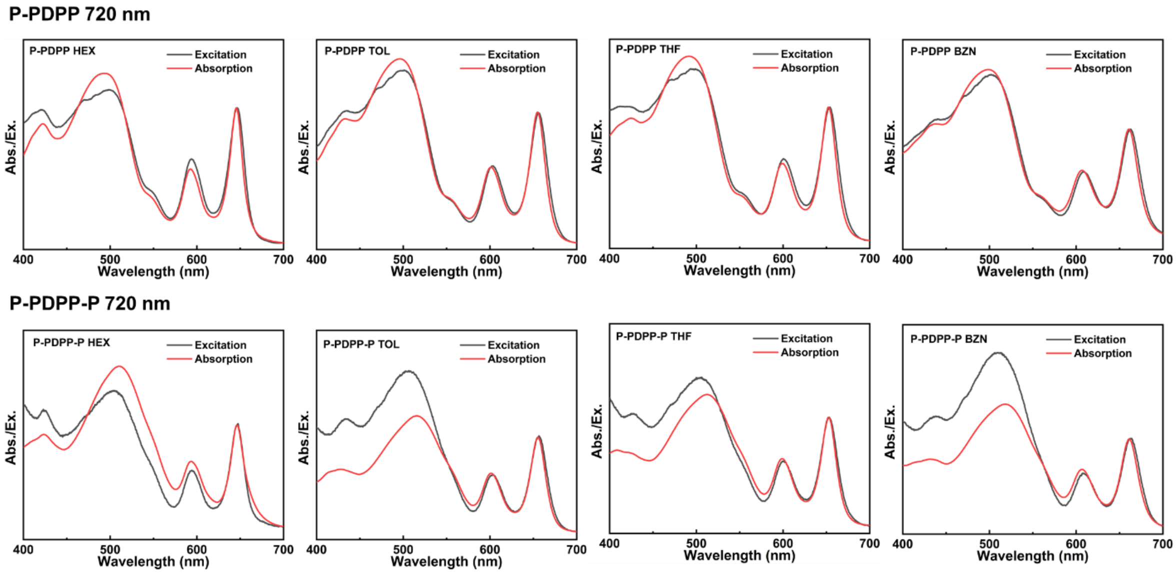

Fig. S11. The excitation spectra of **P-PDPP** and **P-PDPP-P** in different solvents.

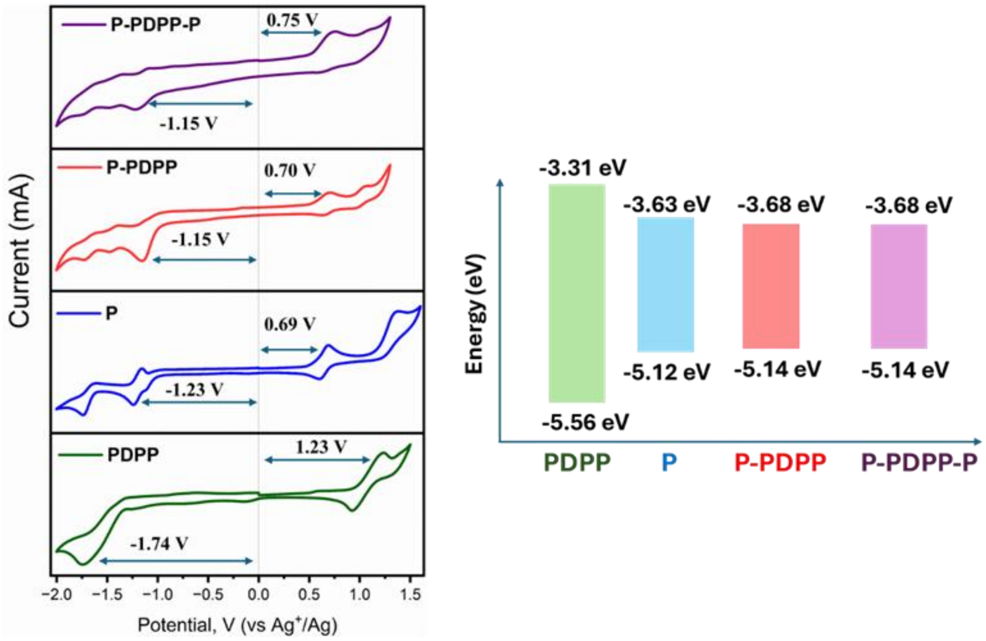

Fig. S12. Cyclic voltammograms of PDPP, P, **P-PDPP**, **P-PDPP-P** and the molecular energy level diagram obtained through cyclic voltammetry.

Table S2. The PLQY of P, PDPP, **P-PDPP** and **P-PDPP-P** in different solvents.

solvents	PDPP (@ 540 nm, lifetime, PLQY)	P (@ 660 nm, lifetime, PLQY)	P-PDPP (@ 670 nm, lifetime, PLQY)		P-PDPP-P (@ 670 nm, lifetime, PLQY)	
HEX	5.1 ns，85%	19.8 ns, 71%	3.0 ns (τ_{avg})[a], 10%	PDPP: 2% P: 8%	2.4 ns, 5%	PDPP: 2% P: 3%
TOL	5.7 ns，89%	15 ns, 45%	6.2 ns, 18%	PDPP: 3% P: 15%	4.1 ns, 4%	PDPP: 1% P: 3%
THF	6.0 ns，94%	14 ns, 36%	4.9 ns, 16%	PDPP: 5% P: 11%	3.6 ns, 4%	PDPP: 2% P: 2%
BZN	6.1 ns，97%	10 ns, 23%	6.1 ns, 17%	PDPP: 5% P: 12%	4.6 ns, 6%	PDPP: 2% P: 4%

[a] Owing to the conformational flexibility of the P–PDPP structure in the excited state, a long-lived minor component emerges in the low-polarity solvent hexane (HEX), where solvation effect is weak. The resulting decay kinetics closely resemble the nanosecond transient absorption dynamics observed for P–PDPP. Lifetime fitting of P–PDPP in HEX yields two decay components: $\tau_1 \approx 2.7$ ns (96.4%) and $\tau_2 \approx 11$ ns (3.6%), giving an average lifetime of approximately 3 ns.

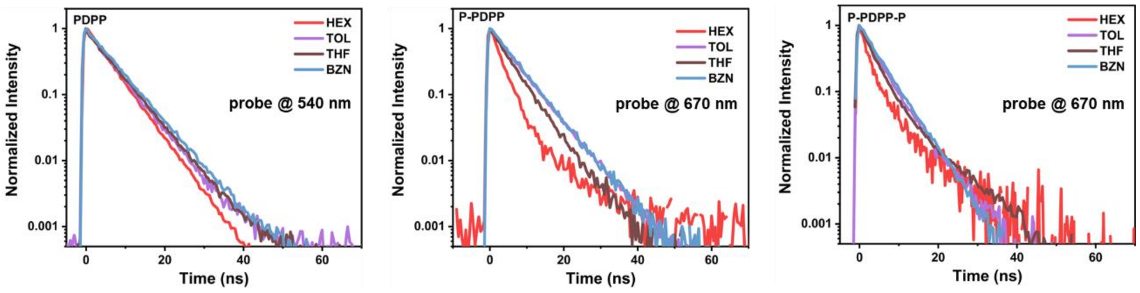

Fig. S13. The PL decay profile of PDPP, P-PDPP and P-PDPP-P in different solvents.

S4. Theoretical Calculations

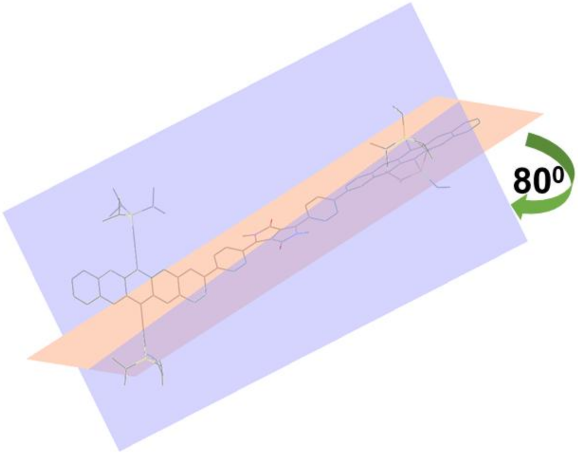

Fig. S14. The optimized geometric structures of P-PDPP-P by applying the DFT calculation.

Table S3. The vertical excitation energies of different optimized structures (three additional) obtained by changing the dihedral angle of the pentacene in the P-PDDP-P system.

	P-PDPP-P-2			**P-PDPP-P-3**			**P-PDPP-P-4**		
dihedral angle	1.4°			79°			2°		
Excited state	$S_0 \rightarrow S_1$	$S_0 \rightarrow S_2$	$S_0 \rightarrow S_3$	$S_0 \rightarrow S_1$	$S_0 \rightarrow S_2$	$S_0 \rightarrow S_3$	$S_0 \rightarrow S_1$	$S_0 \rightarrow S_2$	$S_0 \rightarrow S_3$
Energy (eV)	2.0252ev 612.21nm	2.0277ev 611.45nm	2.7387ev 452.71nm	2.0252ev 612.21nm	2.0279ev 611.39nm	2.7415ev 452.25nm	2.0245ev 612.42nm	2.0287ev 611.15nm	2.7366ev 453.06nm
f (oscillator strength)	0.1636	0.3201	1.7435	0.2173	0.2491	1.6287	0.0626	0.407	1.6863
Orbital contribution	H-1 → L 58.7%, H-1 → L+1 16.2%, H → L+1 13.2%, H → L 9.2%	H → L+1 47.3%, H → L 27.8%, H-1 → L+1 20.8%	H-2 → L+2 58.3%, H-2 → L 20.9%, H → L+2 11.2%	H-1 → L+1 41.3%, H → L 38.6%, H-1 → L 13.2%	H → L+1 45.0%, H-1 → L 35.8%, H → L 9.6%, H-1 → L+1 6.8%	H-2 → L+2 59.4%, H-2 → L 21.1%, H → L+2 12.2%	H-1 → L+1 42.0%, H → L 39.3%, H-1 → L 14.9%	H → L+1 53.7%, H-1 → L 39.7%	H-2 → L+2 58.0%, H-2 → L 21.6%, H → L+2 11.8%

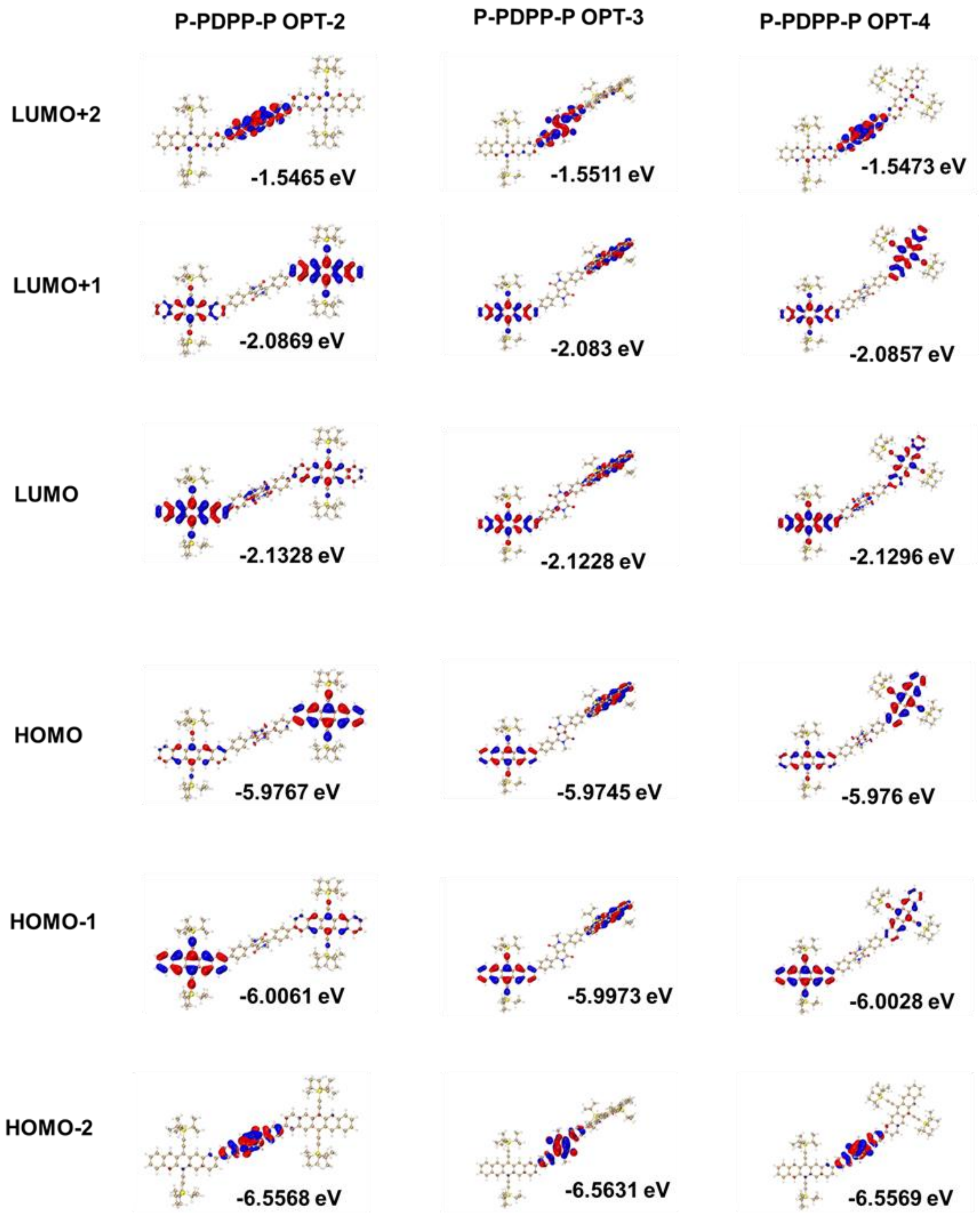

Fig. S15. The frontier molecular orbitals of **P-PDPP-P** based on different optimized ground-state states. The isovalue is set as 0.02.

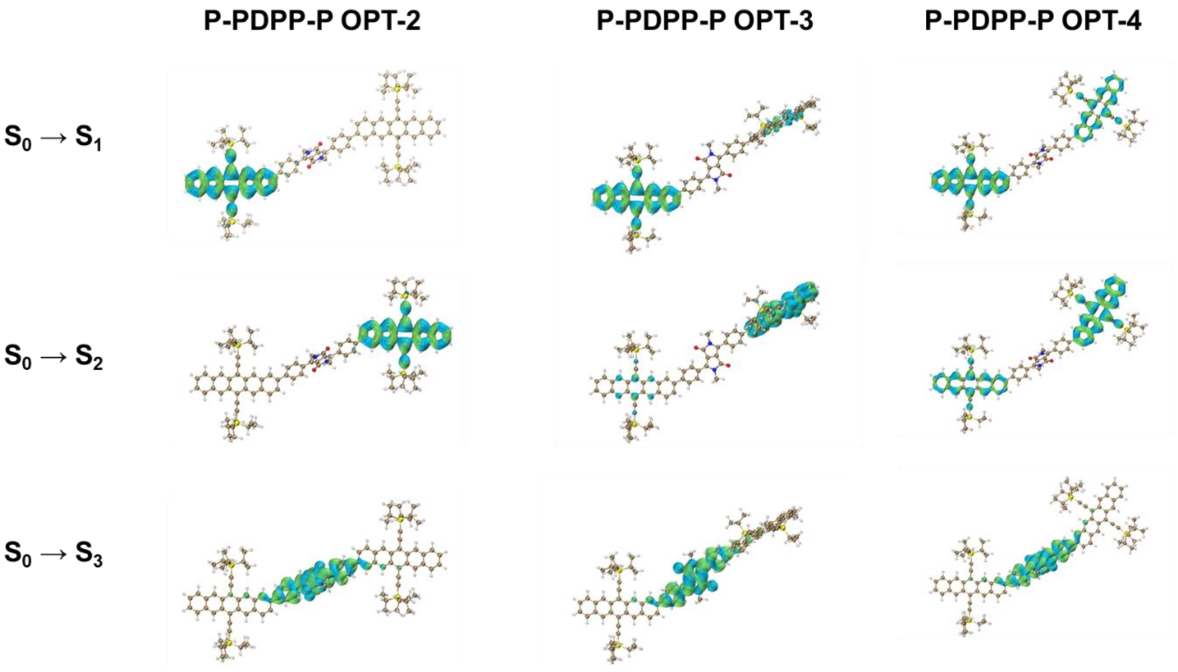

Fig. S16. The excited state electron-hole analysis of different **P-PDPP-P** optimized structures. The isovalue is set as 0.0004. The green and blue denote the electron and hole, respectively.

Table S4. Dihedral angle between the phenyl and diketopyrrolopyrrole

molecular	θ_1	θ_2
PDPP	33	32
P-PDPP	29	29
P-PDPP-P	27	27

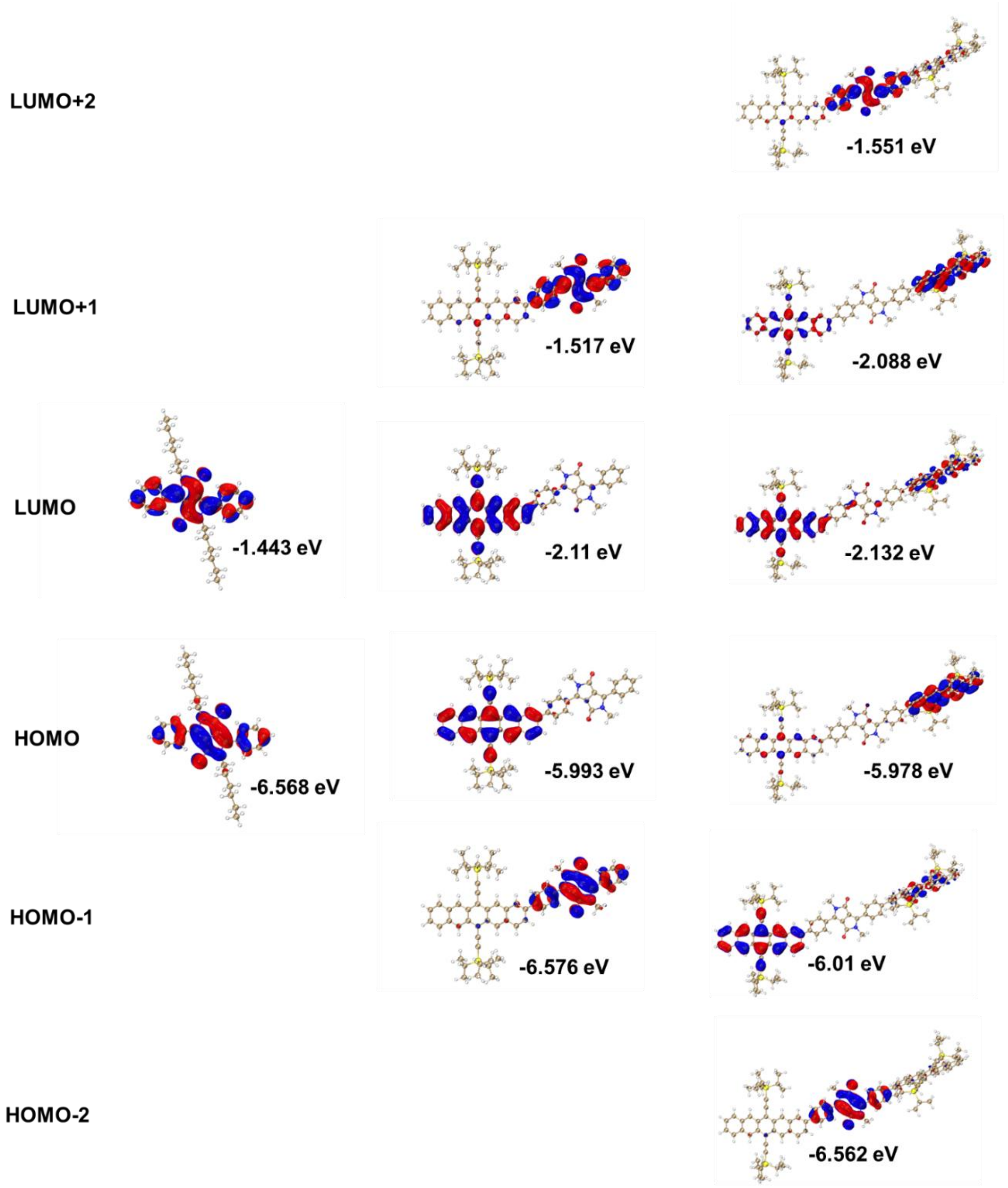

Fig. S17. The frontier molecular orbitals of PDPP, P-**PDPP** and **P-PDPP-P** based on optimized ground-state states. The isovalue is set as 0.02.

Table S5. HOMO-LUMO energy level gap of PDPP segment

molecular	HOMO of PDPP segment eV	LUMO of PDPP segment eV	LUMO-HOMO gap eV
PDPP	-6.568	-1.443	5.125
P-PDPP	-6.576	-1.517	5.059
P-PDPP-P	-6.562	-1.551	5.011

Table S6. The theoretical parameters of excited states for P, PDPP, **P-PDPP**, and **P-PDPP-P**

	P	PDPP	P-PDPP		P-PDPP-P		
Excited state	$S_0 \rightarrow S_1$	$S_0 \rightarrow S_1$	$S_0 \rightarrow S_1$	$S_0 \rightarrow S_2$	$S_0 \rightarrow S_1$	$S_0 \rightarrow S_2$	$S_0 \rightarrow S_3$
Energy (eV)	2.045 (606 nm）	2.943 （421 nm）	2.026 (612 nm)	2.844 (436 nm)	2.027 (612 nm)	2.028 (611 nm)	2.743 (452 nm)
f (oscillator strength)	0.274	0.484	0.249	1.012	0.3044	0.1826	1.752
Orbital contribution	HOMO→LUMO,100%	HOMO→LUMO, 99.1%	HOMO→LUMO, 98%	H-1 → L+1 76.1%, H-1 →L 13.0%, H → L+1 7.4%	H-1 → L 34.7%, H-1 → L+1 34.4%, H → L 26.8%	H → L+1 60.6%, H-1 → L 27.2%, H → L 8.4%	H-2 → L+2 59.4%, H-2 → L 20.0%, H → L+2 10.8%

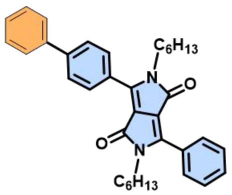

phPDPP

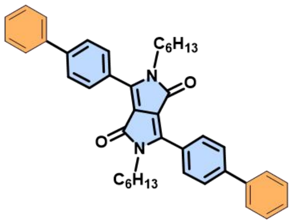

phPDPPph

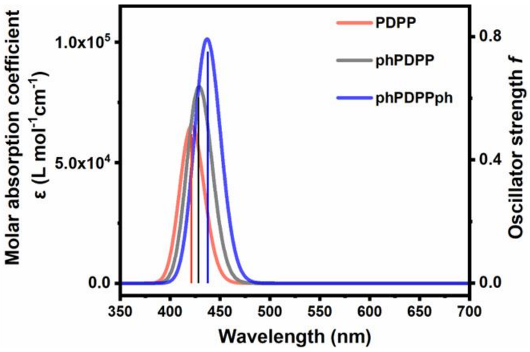

Fig. S18. A. Simulated absorption spectrum of PDPP, phPDPP, and phPDPPph.

Table S7. The theoretical parameters of excited states for PDPP, phPDPP, and phPDPPph

	E_{S1} (eV)	f	orbitals
PDPP	2.943	0.484	H→L (99.1%)
phPDPP	2.89	0.604	H→L (98.4%)
phPDPPph	2.838	0.75	H→L (97.8%)

S5. Transient Absorption Results of PDPP and P-PDPP

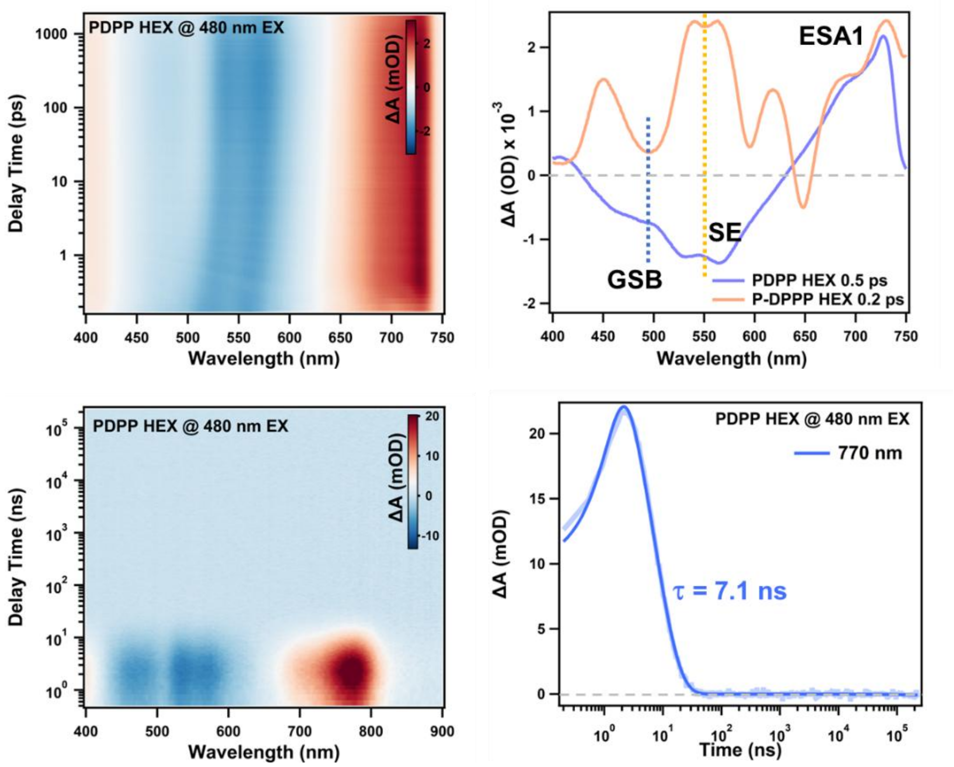

Fig. S19. fs-TA and ns-TA results of PDPP in HEX.

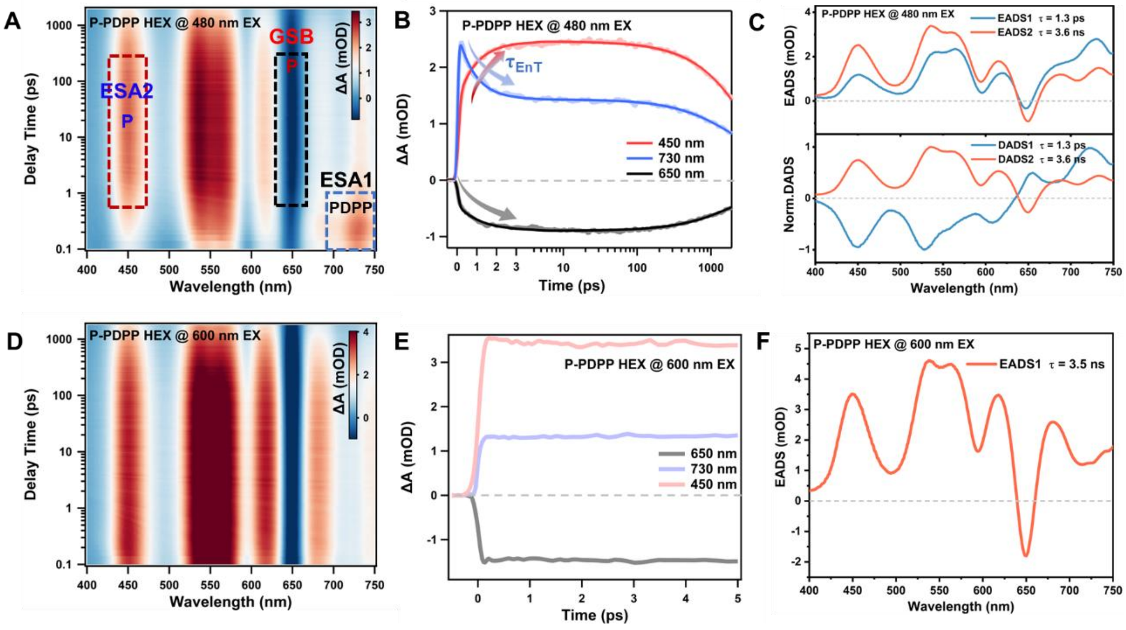

Fig. S20. fs-TA heat maps of **P-PDPP** in HEX at 480/600 nm (A, D) excitation, selected single wavelength kinetics traces (B, E), and evolution/different associated difference spectra (C, F) obtained from global analysis.

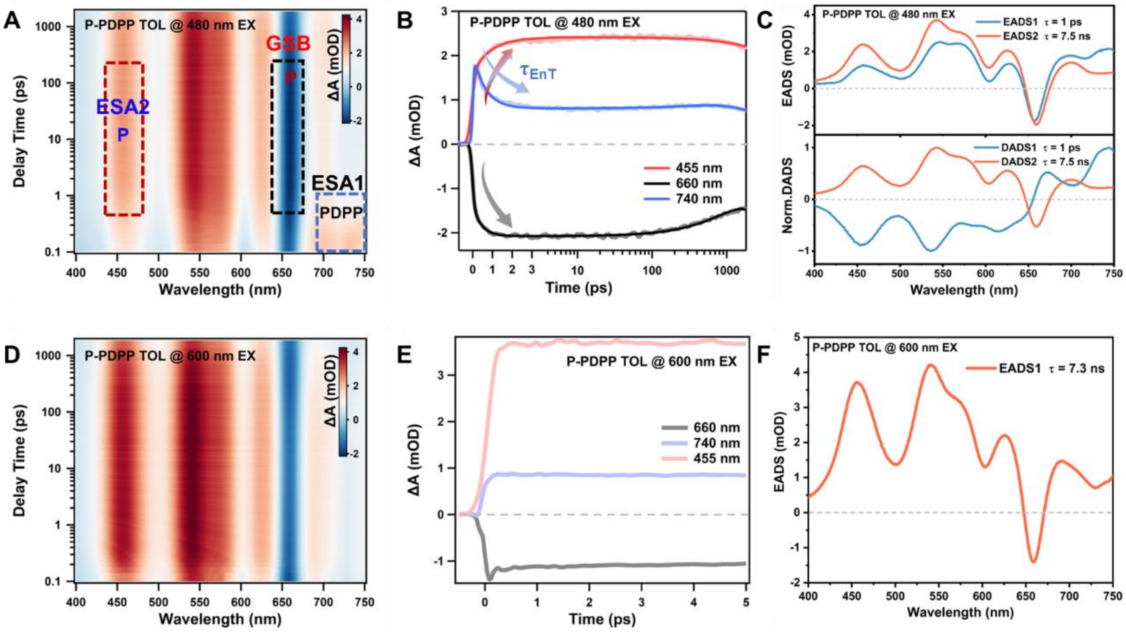

Fig. S21. fs-TA heat maps of **P-PDPP** in TOL at 480/600 nm (A, D) excitation, selected single wavelength kinetics traces (B, E), and evolution/different associated difference spectra (C, F) obtained from a global analysis.

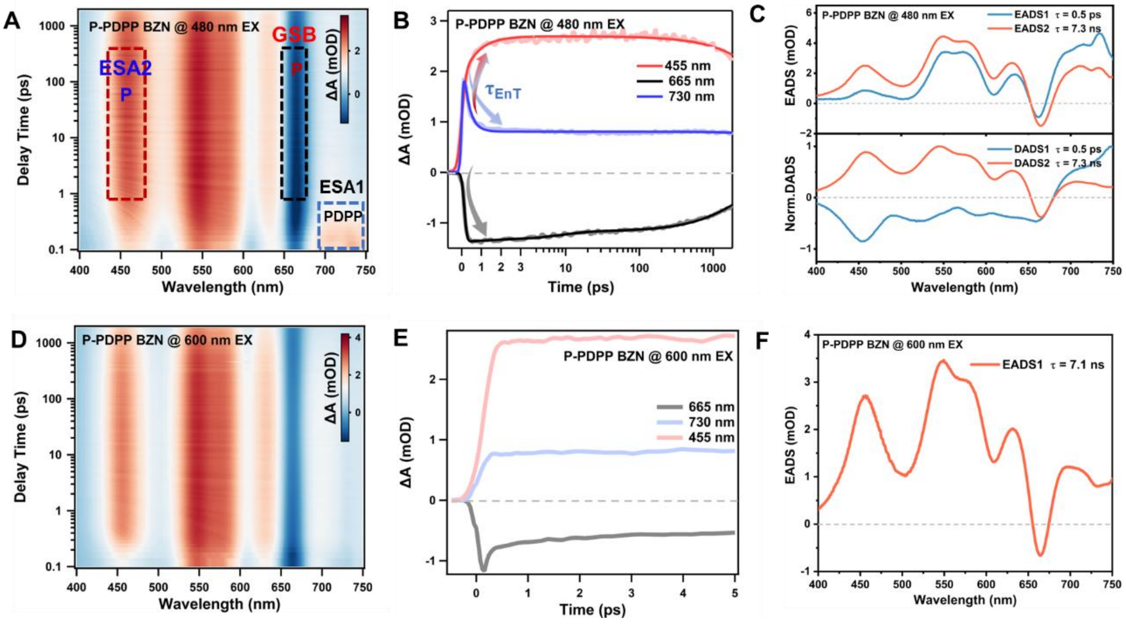

Fig. S22. fs-TA heat maps of **P-PDPP** in BZN at 480/600 nm (A, D) excitation, selected single wavelength kinetics traces (B, E), and evolution/different associated difference spectra (C, F) obtained from a global analysis.

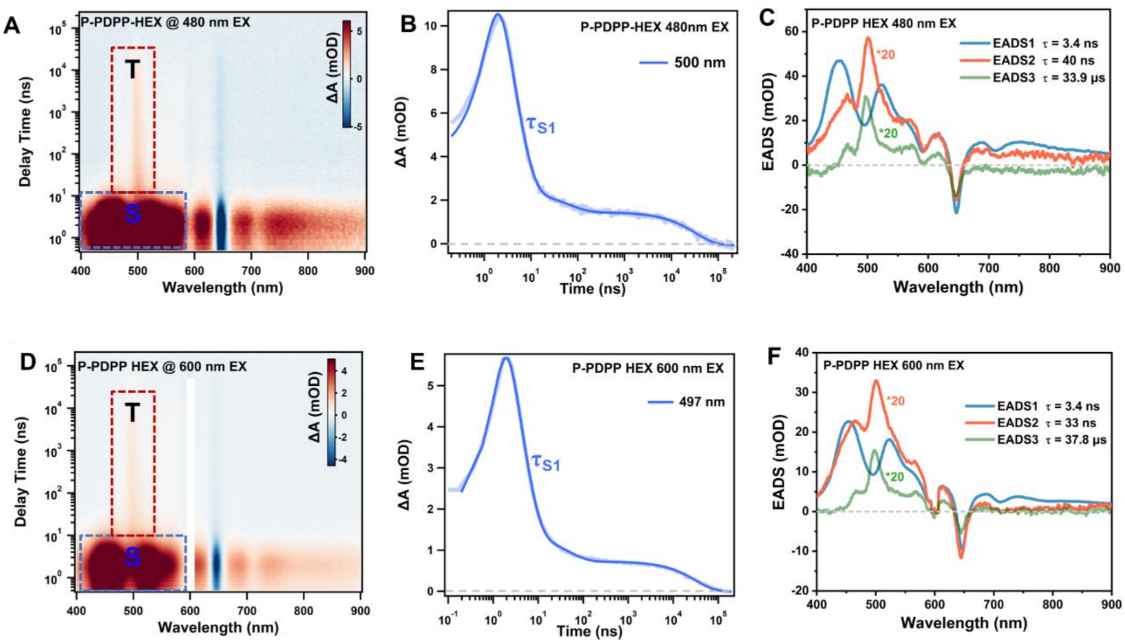

Fig. S23. ns-TA heat maps of **P-PDPP** in HEX at 480/600 nm (A, D) excitation, selected single wavelength kinetics traces (B, E), and evolution associated difference spectra (C, F) obtained from a global analysis. The time constant on the order of several tens of nanoseconds is not observed in other solvents and is therefore attributed to the presence of multiple sub-ensembles, corresponding to S_1 states with distinct electronic and geometric configurations. Within this framework, one sub-ensemble undergoes intersystem crossing to generate triplet excitons; accordingly, the contribution of the resulting T_1 state is included in EADS2.

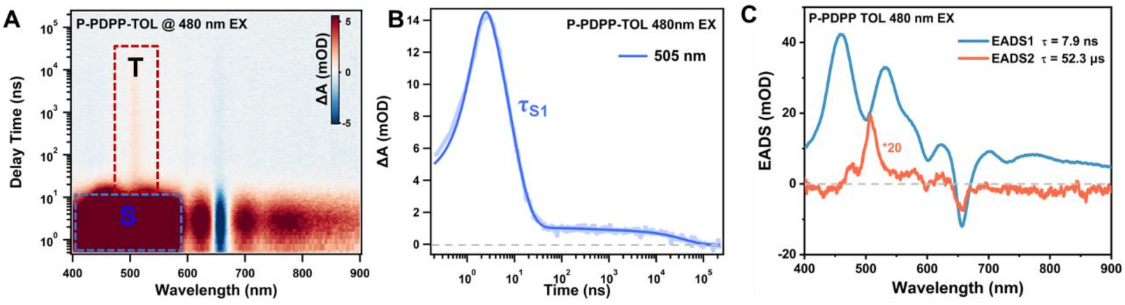

Fig. S24. ns-TA heat map of **P-PDPP** in TOL at 480nm (A) excitation, selected single wavelength kinetics traces (B), and evolution associated difference spectra (C) obtained from a global analysis.

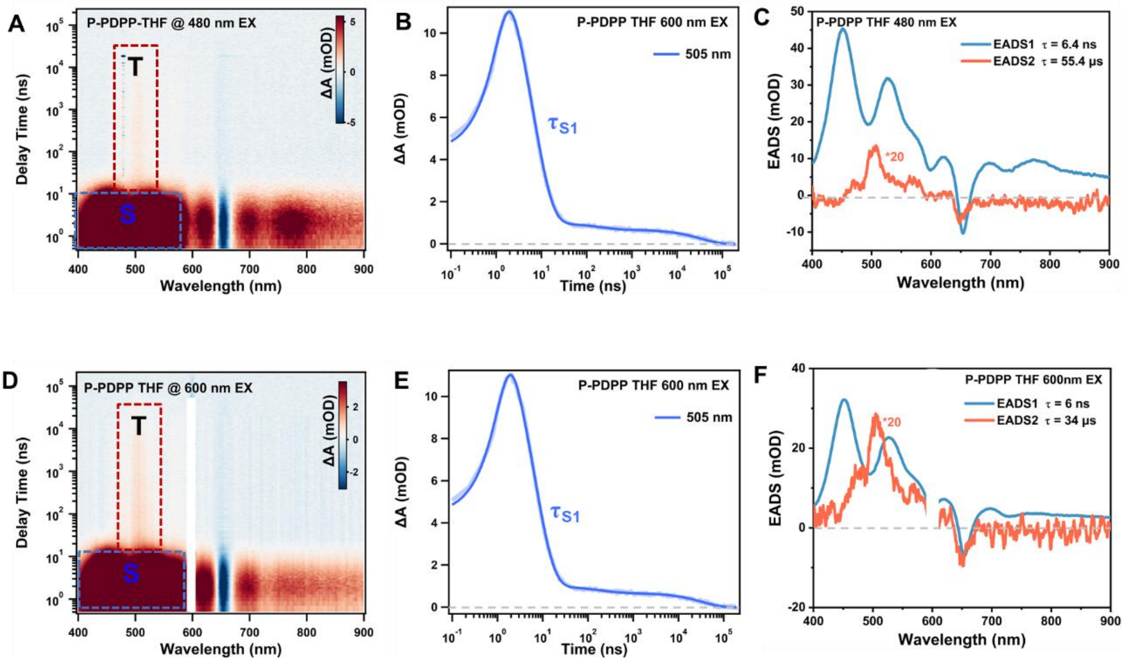

Fig. S25. ns-TA heat maps of **P-PDPP** in THF at 480/600 nm (A, D) excitation, selected single wavelength kinetics traces (B, E), and evolution associated difference spectra (C, F) obtained from a global analysis.

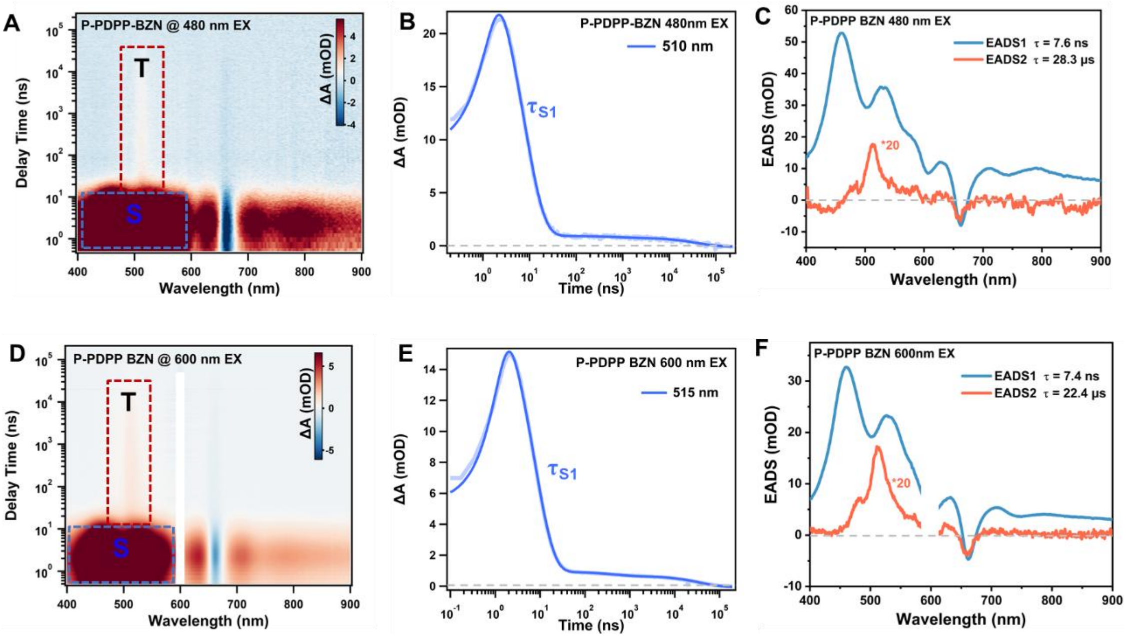

Fig. S26. ns-TA heat maps of P-PDPP in BZN at 480/600 nm (A, D) excitation, selected single wavelength kinetics traces (B, E), and evolution associated difference spectra (C, F) obtained from a global analysis.

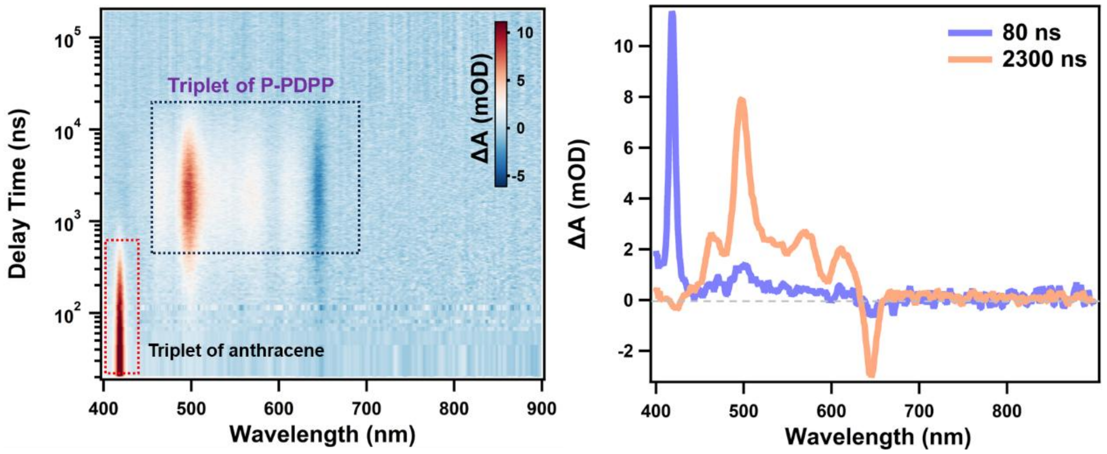

Fig. S27. Sensitization experiment of **P-PDPP** in HEX. sensitizer: anthracene, excitation 360 nm.

S6. FRET calculation on P-PDPP and P-PDPP-P

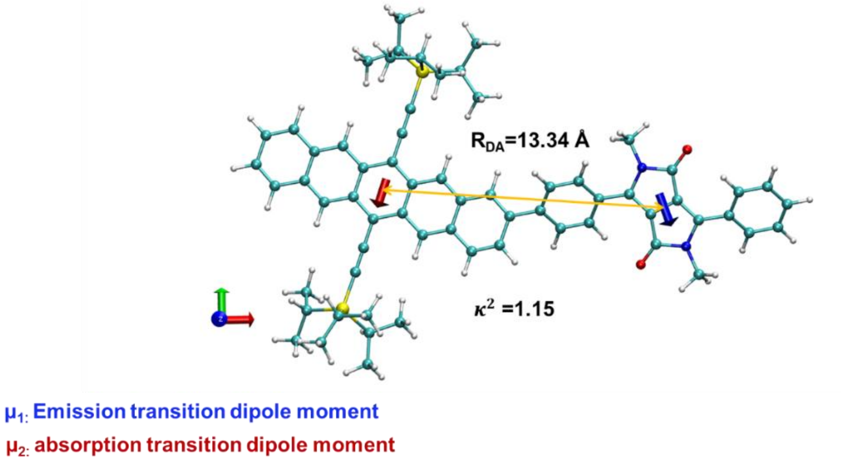

Fig. S28. Computationally transition dipole moments and oriental factor of a **P-PDPP**.

Table S8. Parameters used to calculate the theoretical FRET rate constants of **P-PDPP-P** in different solvents

P-PDPP-P					
	n	J	R_0 (nm)	k_{FRET}(s^{-1})	E
HEX	1.375	2.0931×10^{15}	6.013	1.631×10^{12}	0.9999
TOL	1.496	2.2992×10^{15}	5.878	1.285×10^{12}	0.9999
THF	1.407	2.1716×10^{15}	6.12	1.564×10^{12}	0.9999
BZN	1.528	2.3351×10^{15}	5.894	1.217×10^{12}	0.9999

Comparison between theoretical FRET rate and experimental rate FRET (fs-TA):

Experimental energy-transfer efficiency formula:

$$E = 1 - \frac{\tau_{DA}}{\tau_D}$$

Table S9. The energy transfer rate and efficiency obtained from the fs-TA experiment

	P-PDPP				**P-PDPP-P**			
	k_{FRET} (s^{-1}, fs-TA)	τ_{DA} (ps)	τ_D (ns)	E	k_{FRET} (s^{-1}, fs-TA)	τ_{DA} (ps)	τ_D (ns)	E
HEX	6.25×10^{11}	1.6	5.1	0.9997	1×10^{12}	1	5.1	0.9998
TOL	9.09091×10^{11}	1.1	5.7	0.9998	1.25×10^{12}	0.8	5.7	0.9998
THF	1.25×10^{12}	0.8	6.0	0.9998	2×10^{12}	0.5	6.0	0.9999
BZN	2×10^{11}	0.5	6.1	0.9999	3.33×10^{12}	0.3	6.1	0.9999

S7. Transient Absorption Results of P-PDPP-P

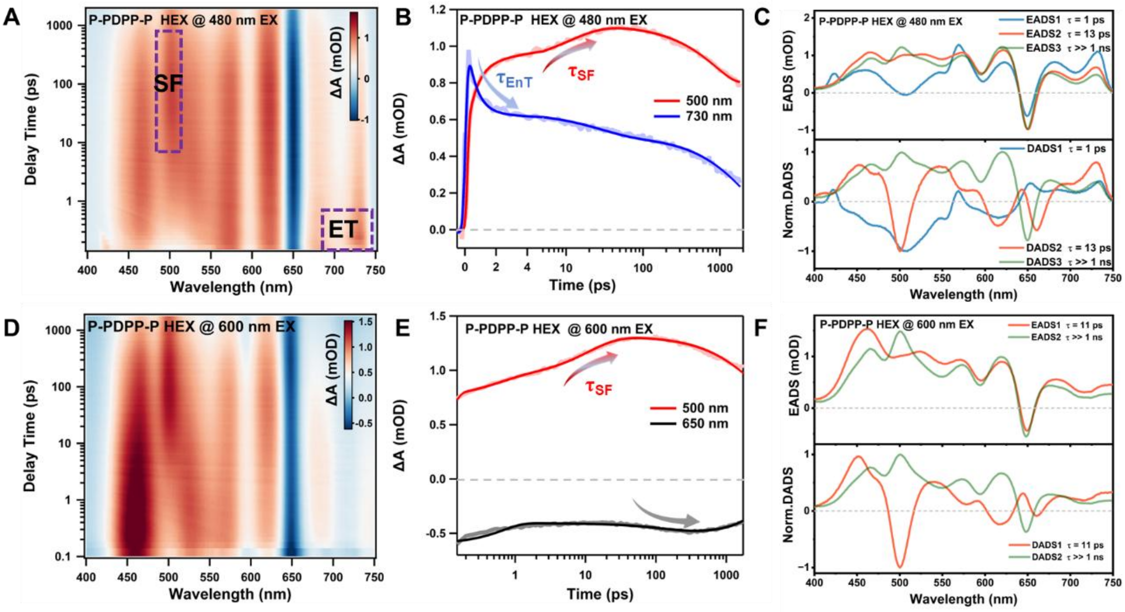

Fig. S29. fs-TA heat maps of **P-PDPP-P** in HEX at 480/600 nm (A, D) excitation, selected single wavelength kinetics traces (B, E), and evolution/different associated difference spectra (C, F) obtained from a global analysis.

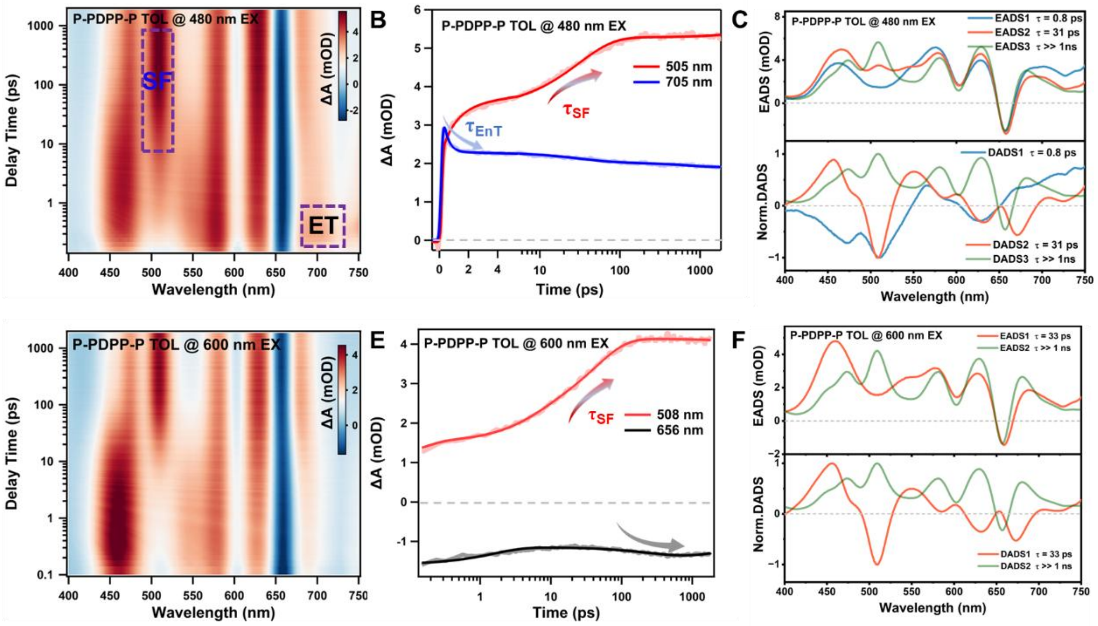

Fig. S30. fs-TA heat maps of **P-PDPP-P** in TOL at 480/600 nm (A, D) excitation, selected single wavelength kinetics traces (B, E), and evolution/different associated difference spectra (C, F) obtained from a global analysis.

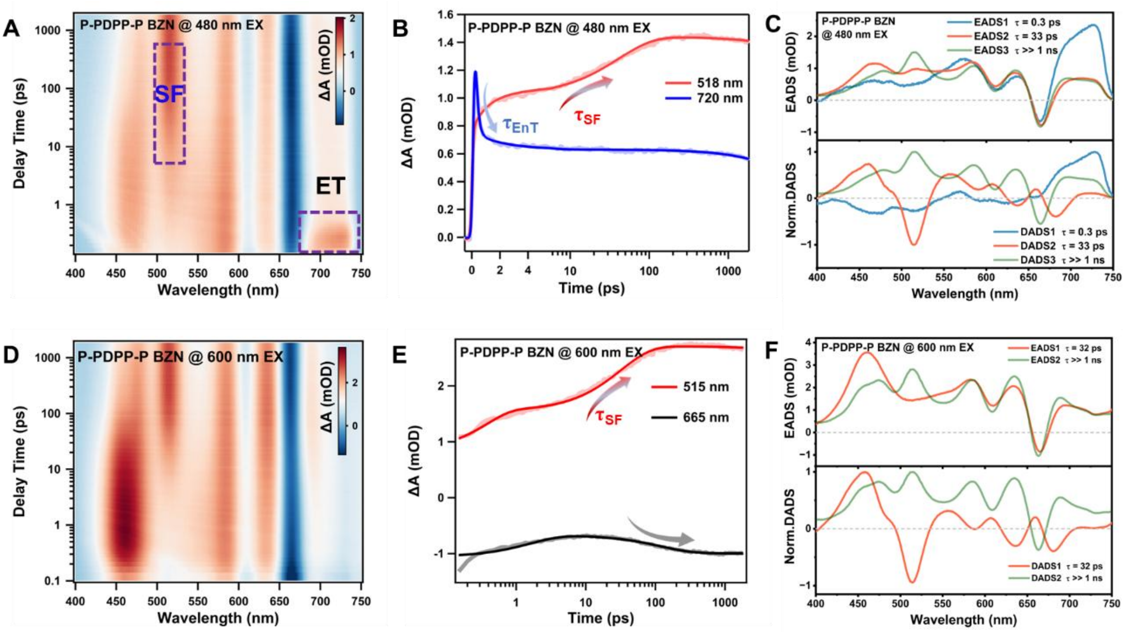

Fig. S31. fs-TA heat maps of **P-PDPP-P** in BZN at 480/600 nm (A, D) excitation, selected single wavelength kinetics traces (B, E), and evolution/different associated difference spectra (C, F) obtained from a global analysis.

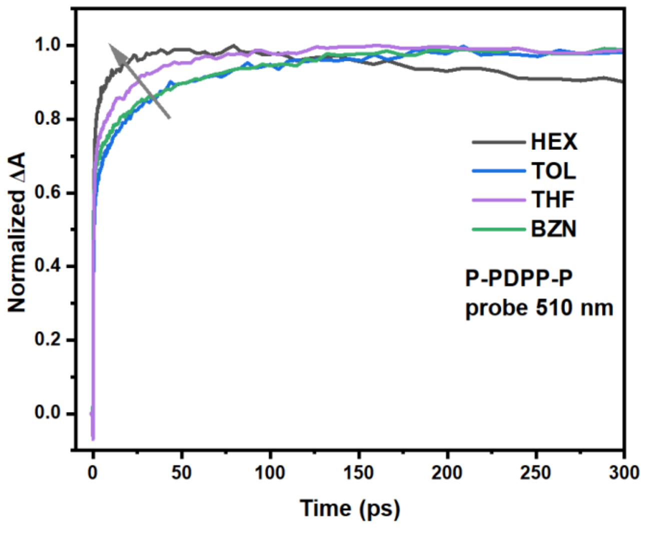

Fig. S32. Comparison of ^{1}(TT) formation kinetics of **P-PDPP-P** in different solvents.

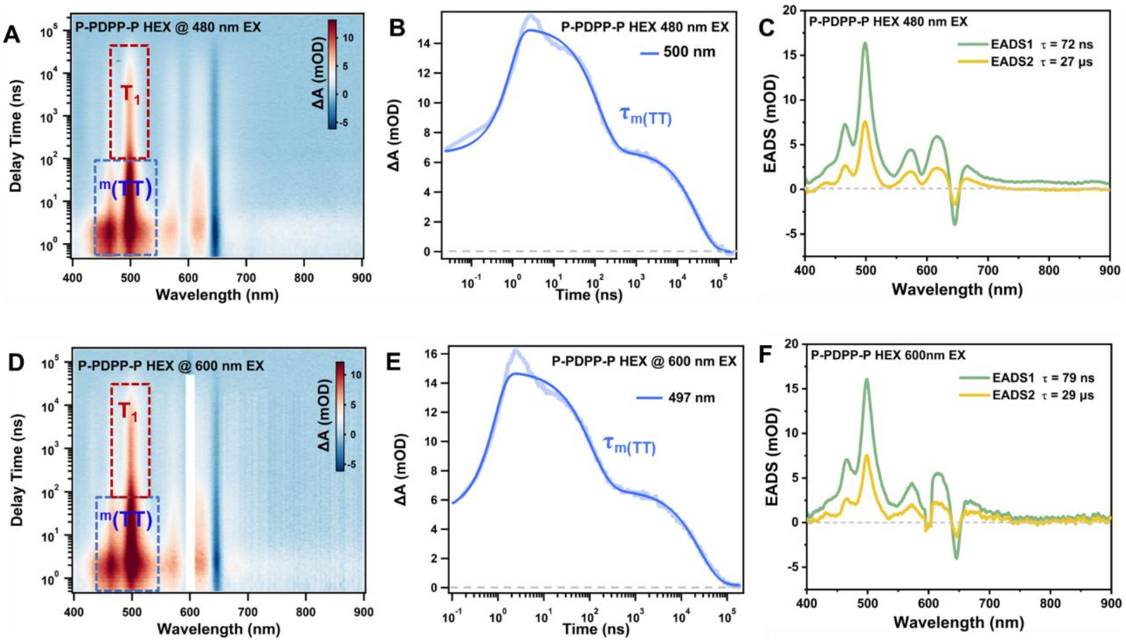

Fig. S33. ns-TA heat maps of **P-PDPP-P** in HEX at 480/600 nm (A, D) excitation, selected single wavelength kinetics traces (B, E), and evolution associated difference spectra (C, F) obtained from a global analysis.

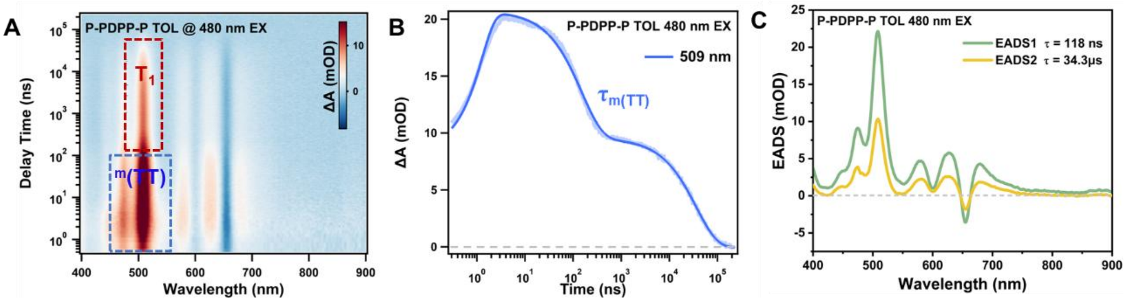

Fig. S34. ns-TA heat maps of **P-PDPP-P** in TOL at 480 nm (A) excitation, selected single wavelength kinetics traces (B), and evolution associated difference spectra (C) obtained from a global analysis.

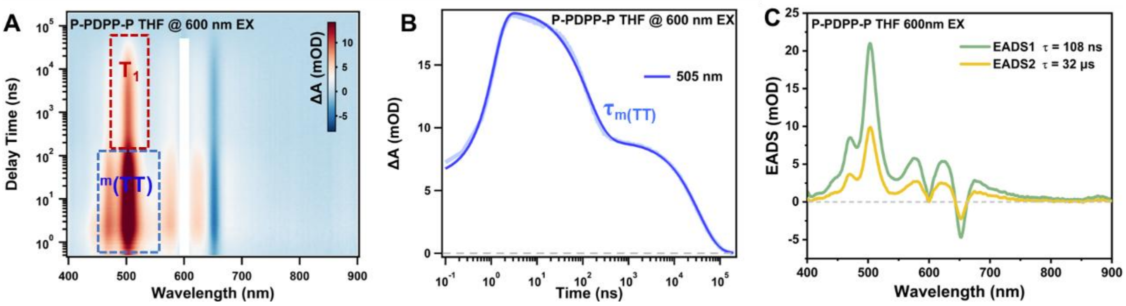

Fig. S35. ns-TA heat maps of **P-PDPP-P** in THF at 600 nm (A) excitation, selected single wavelength kinetics traces (B), and evolution associated difference spectra (C) obtained from a global analysis.

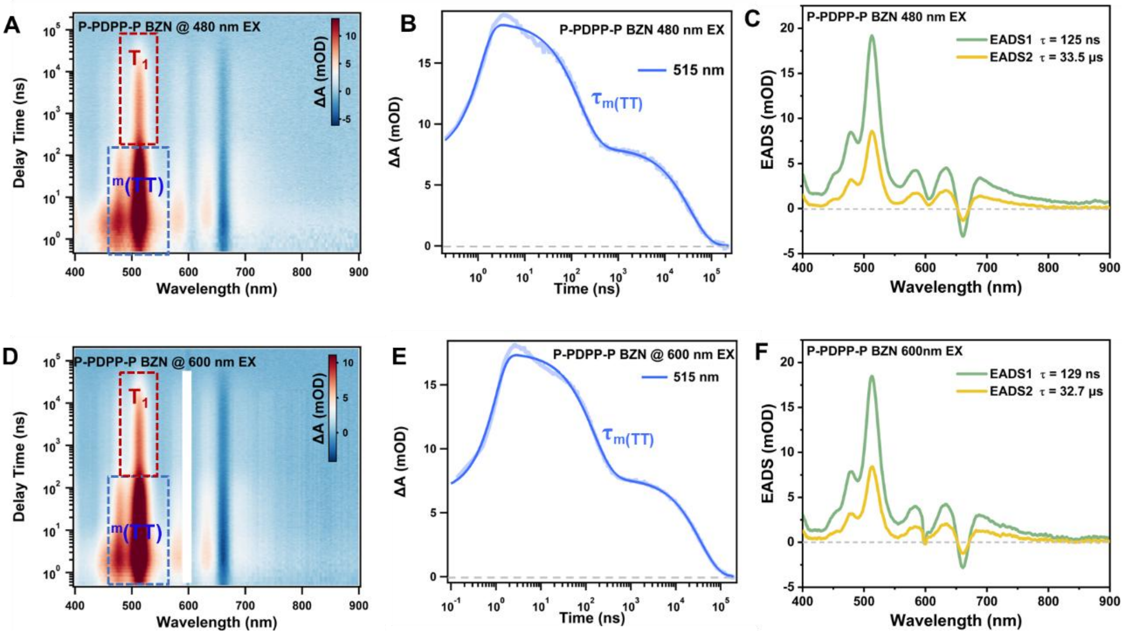

Fig. S36. ns-TA heat maps of **P-PDPP-P** in BZN at 480/600 nm (A, D) excitation, selected single wavelength kinetics traces (B, E), and evolution associated difference spectra (C, F) obtained from a global analysis.

Table S10. Kinetic data from fs-TA and ns-TA measurements for **P-PDPP** and **P-PDPP-P** in different solvent. Here, the T_1 lifetime of P is approximately 30–35 μs, and any smaller or larger extracted values are likely attributable to errors arising from the low signal-to-noise ratio of the data.

Solvent		Pump /nm	S_n (PDPP)	S_1(P)/SF	^{m}(TT)	T_1
HEX	**P-PDPP**	480	1.6 ps	3.4 ns	/	33.9 μs
		600	-	3.4 ns	/	37.8 μs
	P-PDPP-P	480	1 ps	13 ps	72 ns	27 μs
		600	-	11 ps	79 ns	29 μs
TOL	**P-PDPP**	480	1.1 ps	7.5 ns	/	52.3 μs
		600	-	7.3 ns	/	/
	P-PDPP-P	480	0.8 ps	31 ps	118 ns	34.3 μs
		600	-	33 ps		
THF	**P-PDPP**	480	0.8 ps	5.9 ns	/	55.4 μs
		600	-	5.5 ns	/	34 μs

	P-PDPP-P	480	0.5 ps	21 ps	100 ns	32.8 μs
		600	-	22 ps	108 ns	32 μs
BZN	**P-PDPP**	480	0.5 ps	7.3 ns	/	28.3 μs
		600	-	7.1 ns	/	22.4 μs
	P-PDPP-P	480	0.3 ps	33 ps	125 ns	33.5 μs
		600	-	32 ps	129 ns	32.7 μs

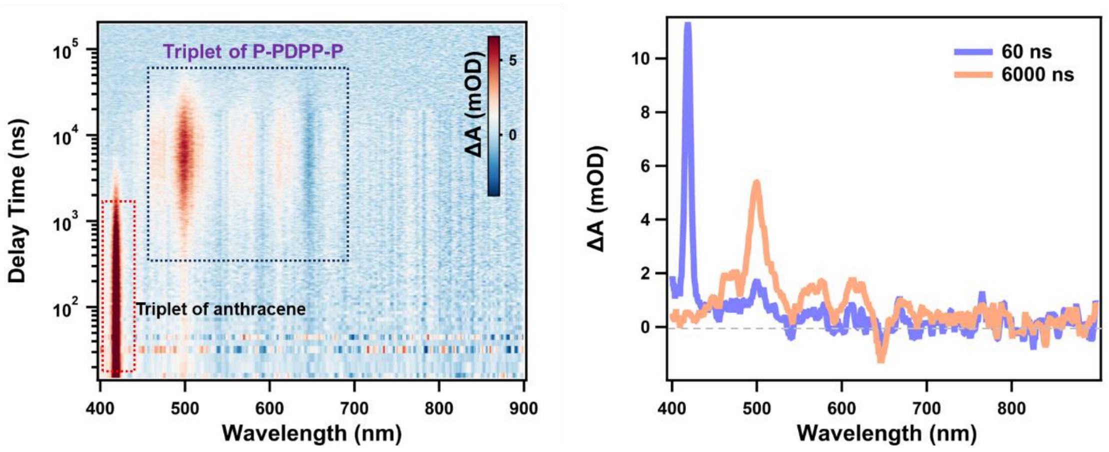

Fig. S37. Sensitization experiment of **P-PDPP-P** in HEX. sensitizer: anthracene, excitation 360 nm.

S8. References

1. M. J. Frisch, G. W. Trucks, H. B. Schlegel, G. E. Scuseria, M. A. Robb, J. R. Cheeseman, G. Scalmani, V. Barone, G. A. Petersson, H. Nakatsuji, X. Li, M. Caricato, A. V. Marenich, J. Bloino, B. G. Janesko, R. Gomperts, B. Mennucci, H. P. Hratchian, J. V. Ortiz, A. F. Izmaylov, J. L. Sonnenberg, Williams, F. Ding, F. Lipparini, F. Egidi, J. Goings, B. Peng, A. Petrone, T. Henderson, D. Ranasinghe, V. G. Zakrzewski, J. Gao, N. Rega, G. Zheng, W. Liang, M. Hada, M. Ehara, K. Toyota, R. Fukuda, J. Hasegawa, M. Ishida, T. Nakajima, Y. Honda, O. Kitao, H. Nakai, T. Vreven, K. Throssell, J. A. Montgomery Jr., J. E. Peralta, F. Ogliaro, M. J. Bearpark, J. J. Heyd, E. N. Brothers, K. N. Kudin, V. N. Staroverov, T. A. Keith, R. Kobayashi, J. Normand, K. Raghavachari, A. P. Rendell, J. C. Burant, S. S. Iyengar, J. Tomasi, M. Cossi, J. M. Millam, M. Klene, C. Adamo, R. Cammi, J. W. Ochterski, R. L. Martin, K. Morokuma, O. Farkas, J. B. Foresman and D. J. Fox, Gaussian 16 Rev. C.01. *Wallingford CT,* 2016.
2. K. Okuno, Y. Shigeta, R. Kishi, H. Miyasaka and M. Nakano, *J. Photochem. Photobiol. A: Chem.*, 2012, **235**, 29-34.
3. B. P. Pritchard, D. Altarawy, B. Didier, T. D. Gibson and T. L. Windus, *J. Chem. Inf. Model.*, 2019, **59**, 4814-4820.
4. T. Lu and F. Chen, *J. Comput. Chem.*, 2012, **33**, 580-592.
5. W. Humphrey, A. Dalke and K. Schulten, *Journal of Molecular Graphics*, 1996, **14**, 33-38.
6. A. M. Brouwer, 2011, **83**, 2213-2228.
7. J. J. Snellenburg, S. Laptenok, R. Seger, K. M. Mullen and I. H. M. van Stokkum, *J. Stat. Soft.*, 2012, **49**, 1 - 22.
8. A. Cravcenco, C. Ye, J. Gräfenstein and K. Börjesson, *J. Phys. Chem. A*, 2020, **124**, 7219-7227.
9. A. R. Clapp, I. L. Medintz, J. M. Mauro, B. R. Fisher, M. G. Bawendi and H. Mattoussi, *J. Am. Chem. Soc.*, 2004, **126**, 301-310.
10. J. Dhar, N. Venkatramaiah, A. A and S. Patil, *J. Mater. Chem. C*, 2014, **2**, 3457-3466.
11. S. N. Sanders, E. Kumarasamy, A. B. Pun, M. T. Trinh, B. Choi, J. Xia, E. J. Taffet, J. Z. Low, J. R. Miller, X. Roy, X. Y. Zhu, M. L. Steigerwald, M. Y. Sfeir and L. M. Campos, *J. Am. Chem. Soc.*, 2015, **137**, 8965-8972.